Influence of tellurium on physical properties of $ZnIn_2Se_4$ thin films solar cell

H. K. Mahmood*, B. H. Hussein
Department of Physics, College of Education for Pure Science / Ibn Al-Haitham, University of Baghdad, Baghdad, Iraq

$ZnIn_2(Se_{1-x}Te_x)_4$ (ZIST) chalcopyrite semiconductor thin films at various contents (x = 0.0, 0.2, and 0.4) are deposited on glass and p type silicon (111) substrate to produce heterojunction solar cell by using the thermal evaporation technique at RT where the thickness of 500 nm with a vacuum of 1×10^{-5} mbar and a deposited rates of 5.1 nm/s. This study focuses on how differing x content effect on the factors affecting the solar cell characteristics of ZIST thin film and n-ZIST/p-Si heterojunction. X-ray diffraction XRD investigation shows that this structure of ZIST film is polycrystalline and tetragonal, with (112) preferred orientation at $2\theta \approx 27.01$. Moreover, atomic force microscopy AFM is studying the external morphology of film, and it is shown that both surface roughness and average diameter increase with increasing x content, hence increasing the crystallite size of thin films. UV/visible spectrophotometer was analyse the optical features of ZIST films, such as absorption coefficient, optical energy, and these films possessed a direct gap that decreased with increase of x content until it reached its lowest value of 1.6 eV at x = 0.4. Hall measurement displayed that the ZIST thin film is n-nature semiconductors with a maximum carrier concentration $N_H = 6.2 \times 10^{18}$ ($1/cm^3$), minimum resistivity 0.047 Ω.cm. The illumination current-voltage characteristics revealed that the n-ZIST/p-Si solar cell heterojunction at x = 0.4 content has a maximum efficiency of 2.97%.

(Received June 5, 2024; Accepted September 3, 2024)

Keywords: n-ZIST/p-Si heterojunction, Thin film, Photovoltaic, XRD, Electrical properties

1. Introduction

Heterojunctions that combine crystalline and amorphous semiconductors have been extensively studied and have attracted significant attention because of their high potential in a variation of applications [1-3], for example solar cell, light-emitted diodes, photodetectors, injection lasers, etc. [4]. Zinc indium selenide $ZnIn_2Se_4$ is a ternary chalcopyrite semiconductor that included to $A^{II}B_2^{III}C_4^{VI}$ group. ZIS semiconductor thin films have been considered due to their significant technical application, including solar cell and opto-electronic device [5]. The crystal structure for ZIS is a tetragonal where lattice parameters a and c equal to 5.7095 Å, 11.449 Å respectively [6]. Various methods are used to production ZIS thin films, for example the thermal evaporation technique [7], the flash evaporation technique [8], the spray pyrolysis technique [9], the chemical transport method [10], the chemical bath technique [11], the chemical vapor deposition technique [12], and the electrodeposition technique[13]. ZIS has an energy gap type direct ranging (2-2.2) eV [14] and a high absorption coefficient (10^3-10^5) cm^{-1}[15, 16].

ZIS is suitable for optoelectronic applications due to its high photoelectric sensitivity, which ranges from the visible to the near infrared spectrum [15,17]. The conductivity of ZIS semiconductors is n-type [9, 18], and has a high electrical conductivity at low temperatures [19], with electron mobility of 8×10^7 $cm^2/V.s$ [20]. Several researchers have investigated ZIS thin films. Güllü et al. prepared ZIS thin films using the thermal evaporation technique in a nitrogen environment at varying annealing temperatures. The optical tests reveal that the optical absorption coefficients are 10^4 cm^{-1}, and the optical energy gap ranges between 2.52 and 2.26 eV [21]. Dhruv et al. deposited ZIS thin films by flash-evaporation on substrates (glass and pyrographite). I-V properties of the memory devices were investigated at various annealing temperatures [22]. El-Nahass, et al. deposited ZIS thin films onto substrates made of glass using the thermal evaporation method. The XRD pattern of the films displays a structure of nanocrystalline with (112) plane

Corresponding author: hesham.kamel2204p@ihcoedu.uobaghdad.edu.iq
https://doi.org/10.15251/CL.2024.219.687

orientation, the maximum barrier height was found to be 0.4 eV [7]. Babu et al. was studying the effects of the pH on properties of ZIS thin film by using the chemical technique. The XRD displays that the film has a poly-crystalline structures, with a preferred (112) orientation. The optical gap ranged from (2.15 to 2.64) eV [11]. Choe, Sung-Hyu employed the vertical Bridgman method to investigate the optical gaps of un-doped and (Co) doped ZIS single crystals. The measurements showed the energy gaps were direct given by 1.77 eV for the un-doped ZIS and 1.41 eV for the (Co) doped at 300 K [23]. This work focuses on the effect of Te content on the properties of ZIS thin film for the fabrication of (n-ZIST/p-Si) heterojunction solar cell by the using thermal evaporation method and their characterization utilizing optical measurements, XRD, the Hall effect, I-V properties, and the conversion efficiency.

2. Experimental

$ZnIn_2(Se_{1-x}Te_x)_4$ (ZIST) alloys have been produced with a (1:2:4) stoichiometric weighed proportion and a high purity (99.99%) of zinc, indium, selenium, and tellurium, as well as variable concentrations of (x = 0.0, 0.2, and 0.4). these elements are mixed and fused in cleaned ampules of quartz, 22 cm long, with a pressure of 5×10^{-3} mbar. The ampules were heated in an electric-oven at 1273 K for (six hours) before cooling to room temperature (RT) to produce three alloys. It is important to note that the temperature necessary to thoroughly solidify the alloy exceeded the melting points of ZIS and ZIST. The vacuum thermal evaporation technique was utilized to form thin films of ZIST with different contents of (x = 0.0, 0.2, and 0.4) and thicknesses of 500 nm onto well-cleaned glass and p-type silicon (111) substrates to produce solar cell. The rate of deposition of ZIS and ZIST thin films was 5.1 nm/s in a vacuum of 1×10^{-5} mbar. X-ray diffraction (LabX-6000 SHIMADZU Japan) is used for investigate crystal structure of thin film (λ_{Cu,k_α}= 1.5418 Å). Scherer's equation was utilized for determine the crystal size C.S [24-27]:

$$C.S = \frac{0.9 * \lambda}{\beta \cos\theta} \tag{1}$$

The symbol β : the full-width at half-maximum of primary peak, θ: the reflection angles (Barak's angle). Lattice constants a & c for a tetragonal structure are determined using the following equation [28]:

$$\frac{4sin^2\theta}{\lambda^2} = \frac{h^2+k^2}{a^2} + \frac{l^2}{c^2} \tag{2}$$

where (hkl) Miller incidents. AFM technology (Core AFM 2023, Nano. Surf. AG, Switzerland) was used to determine the average diameter, surface morphology, and roughness of thin film materials and found that these parameters are influenced by increasing the x content. The transmittance and reflectance were measured using a UV- spectrophotometer (EMCLAB-61PC) within the 400 to1000 nanometers wavelength. The optical energy gap (E_g^{opt}) and the absorption coefficient (α) were found by using the Tauc equation and the Lambert law, respectively [29-33]:

$$\alpha h\nu = F\,(h\nu - E_g^{opt})^z \tag{3}$$

$$\alpha = \frac{2.303\,A}{t} \tag{4}$$

The symbol (F) is a constant that is dependent on the characteristics of the valence and conduction bands, in addition to the ambient temperature. (hν) represents the magnitude of energy incident photon's. (z): parameter that defines the kind of transition (direct or indirect), where z equals 2 and 0.5 for direct and indirect energy gap, respectively. (A) is the absorption. (t) is the thickness. The Van-der Pauw (Ecopia-HMS-3000) is used for determine the predominant carrier

concentrations, mobility carrier, and carrier type in ZIS and ZIST thin films for Hall effect studies. The features of I-V were calculated using the Shockley equation. Finally, conversion efficiency (η) of solar cell was considered by using the following formal [34, 35]:

$$\eta = \frac{F.F \times J_{sc} \times V_{oc}}{P_{in}} \times 100\% \quad (5)$$

The symbols (J_{sc}),(V_{oc}), and (F. F) are the values of short circuit current density, open circuit voltage, then fill-factor correspondingly. P_{in}: the input power and equals 100 mW/cm^2.

3. Result and discussion

Figure 1 displays the XRD pattern for ZIST thin film with (x = 0.0, 0.2, and 0.4) at RT and thickness 500 nanometers. This Figure show that the ZIST thin films have a polycrystalline tetragonal structure with the (112) preferred orientation at $2\theta \approx 27.01$, and this agrees with the study [36]. Table 1 shows an excellent match between the experimental and standard values on the ICDD 00-039-0458 card. From the same Table, we can observe that the crystallite size increased as x content increased and FWHM decreased. The prepared films reveal an important shift in peak positions with an increase in x content, and that can be due to the slight stress generated by the entry and diffusion of x atoms into the host material and the occupation of sites in the ZIS crystal lattice. We can also be distinguished that as the x content growths, the intensity increases, and this is due to the fact that the crystallinity of the film increases with the increasing in x content [37, 38].

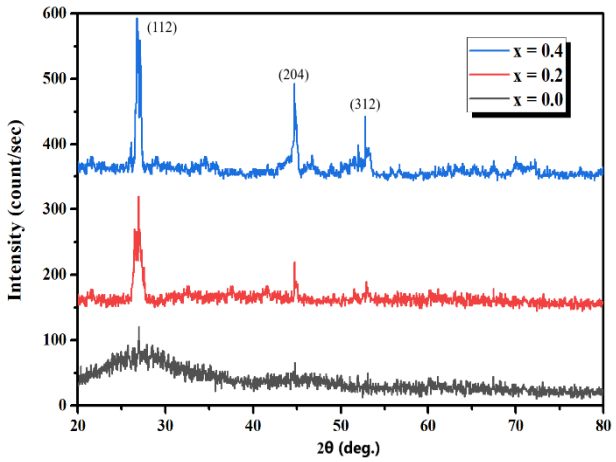

Fig. 1. Pattern of XRD for ZIST thin films with x (0.0, 0.2, and 0.4).

Table 1. XRD data for ZIST thin film at x 0.0, 0.2, and 0.4.

x	d(Å) Std.	d(Å) Exp.	2θ (Deg.) Std.	2θ (Deg.) Exp.	hkl	β (Deg.)	C.S (nm)
ZIST (x = 0.0)	3.29	3.29	27.01	27	(112)	0.82	10.4
	2.01	2.01	44.82	44.82	(204)		
	1.72	1.72	53.15	53.15	(312)		
ZIST (x = 0.2)	3.29	3.29	27.01	27	(112)	0.55	15.51
	2.01	2.02	44.82	44.8	(204)		
	1.72	1.72	53.15	53.08	(312)		
ZIST (x = 0.4)	3.29	3.32	27.01	26.8	(112)	0.28	30.46
	2.01	2.02	44.82	44.76	(204)		
	1.72	1.73	53.15	52.8	(312)		

Figure 2 illustrates three-dimensional 3D images of ZIST thin film at RT and various x contents. From Table 2, we can note that both the roughness and average diameter increase with increasing x content, and that is expected because of the growth in the C.S of thin films. The maximum values reached for both surface roughness and average diameter were 39.16 nm and 96.9 nm at x content equal to (0.4), respectively. Likewise, for the root mean square (r.m.s.), it increases with increase x content until reaching the highest values of 44.69 nm.

Table 2. Aaverage diameter, surfaces roughness, (r.m.s.) for thin films ZIST at RT.

Thin films	Surfaces roughness (nm)	Average diameter (nm)	r.m.s. (nm)
ZIST (x = 0.0)	6.96	19.3	8.43
ZIST (x = 0.2)	19.63	79.99	26.1
ZIST (x = 0.4)	39.16	96.9	44.69

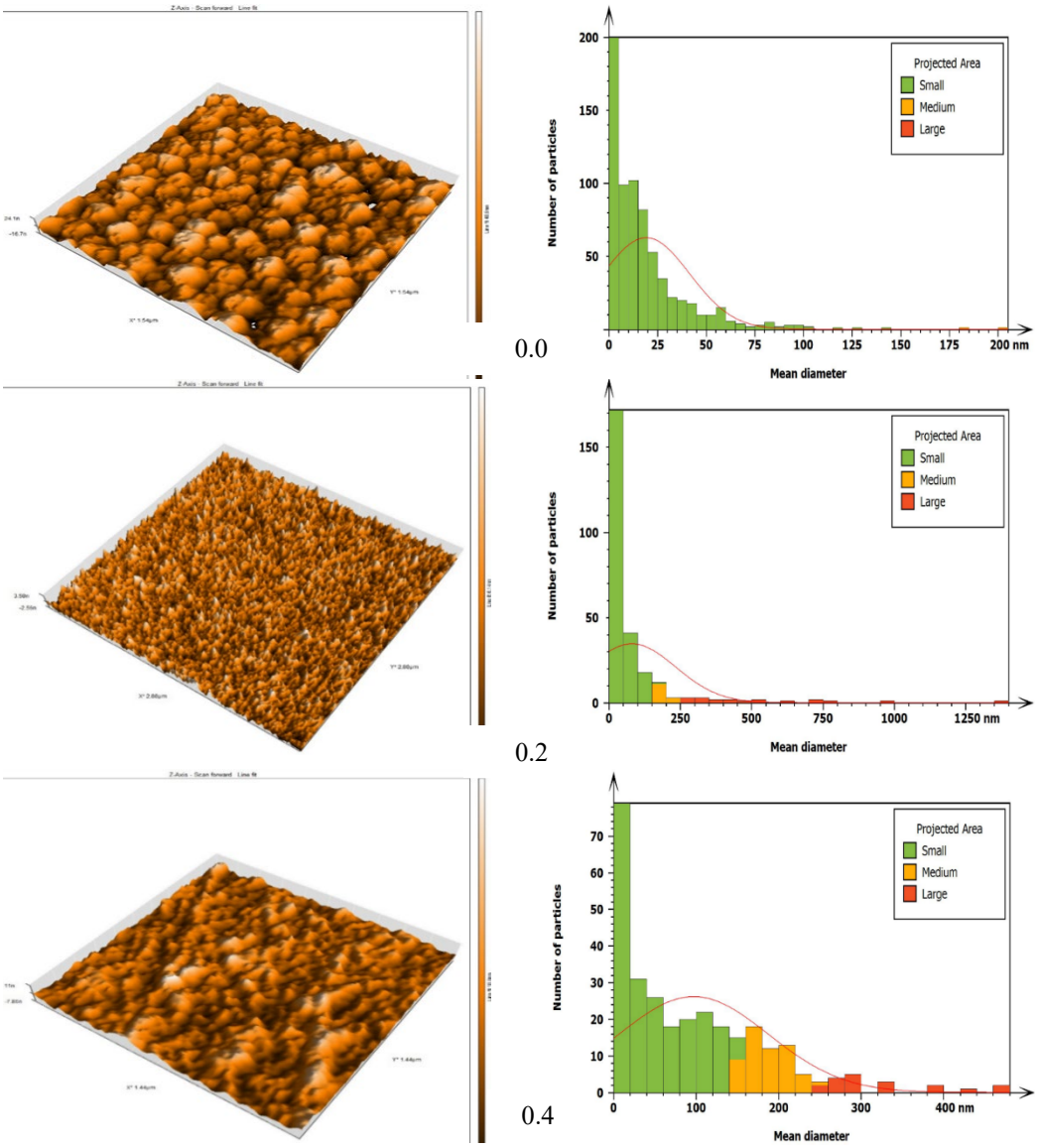

Fig. 2. 3D AFM micrographs of ZIST thin film at x 0.0, 0.2, and 0.4.

Figures 3a and 3b illustrate transmittance and absorbance vs. wavelength, which were measured within the range of 400 nm to 1000 nm. It can be observed that transmittance of ZIST thin film with different contents x 0.0, 0.2, and 0.4 increases with increasing wavelength, in contrast to absorbance, which decreases with increasing wavelength. The greatest absorbance value was attained at a value (x = 0.4) of around 75-80% in the visible band 400-700 nm. Table 3 shows that the absorption coefficient (α) increases with decreasing wavelength, reaching (4×10^4 cm^{-1}) at wavelength (450 nm) and (x = 0.4) content. High absorption coefficient values ($\alpha > 10^4$ cm^{-1}) indicate a direct bandgap. The absorption coefficient acting an important role in defining the ability of a material for absorb the electromagnetic spectrum and, thus, determining the appropriate application for that material. The absorption coefficient of the ZIST thin films increases as we approach the visible spectrum region, as show in Figure 3c. This shows that the film is acceptable for solar cell applications. From Table 3 and Figure 3d, we note clearly that the optical energy gap (E_g^{opt}) decreases as x content increases, eventually reaching 1.6 eV at wavelength 450 nm, and this is expected because of an increasing in the crystalline size resultant from an increase in the average diameter of ZIST thin film material.

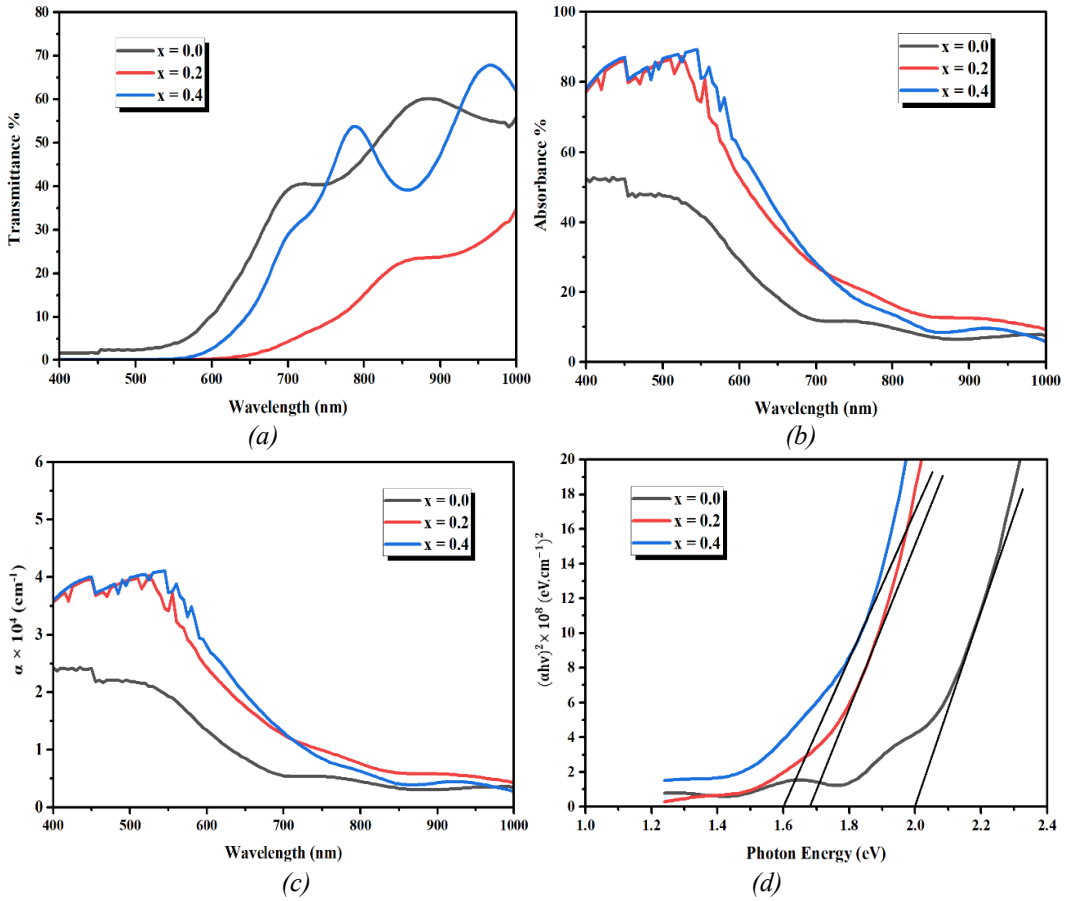

Fig. 3. The transmittance (a), absorbance (b), & absorption coefficient (c) vs. wavelength, $(\alpha h\nu)^2$ (d) vs. photon energy for ZIST thin films at RT.

Table 3. The absorption coefficient and optical band gap (λ= 450 nm) of ZIST thin film at RT.

Thickness (500) nm	E_g^{opt} (eV)	α × 10^4 (cm^{-1})
ZIST (x = 0.0)	2	2.41
ZIST (x = 0.2)	1.68	3.96
ZIST (x = 0.4)	1.6	4

To produce the heterojunction, we need to know the type of thin films p or n-type. The Hall coefficient (R_H) determines the majority carrier type and the mobility (μ_H) of ZIST thin films, which have different x contents at RT. The results obtained showed that all manufactured thin films possess a majority carrier of the negative type, which indicates that these films are of the n-type semiconductor and the carriers are electrons, as in Table 4, and this result is agree with [39]. From the same Table, we can notice that the Hall coefficient (R_H) for ZIST thin films decreases as the carrier concentration (N_H) increases, resulting in an increase in the currents (I) and voltage (V) flowing done the film due to the increasing probability of collision between the carrier's concentration. This means a decrease in resistivity (ρ) and an increase in conductivity (σ) for thin films. The maximum value of (N_H) was reported at (x = 0.4) content equal to (6.2×10^{18} cm^{-3}) at RT.

Table 4. The electrical parameters of ZIST thin films at RT.

Thin films	ρ (Ω.cm)	R_H (cm^3C^{-1})	N_H ($1/cm^3$)	μ_H ($cm^2/V.s$)
ZIST (x = 0.0)	1	-71.8391	8.7×10^{16}	71.83
ZIST (x = 0.2)	0.1	-1.5625	4×10^{18}	15.62
ZIST (x = 0.4)	0.047	-1.00806	6.2×10^{18}	21.16

Figure 4 displays the current density and voltage under the illumination conditions of an n-ZIST/p-Si heterojunction solar cell. From Figure 4, we can detect that the values of the current-density (J) increasing with the increasing in tellurium due to the increasing in the concentrations of N_H. The values of, maximum current density, maximum voltage, short circuit current density, open circuit voltage, fill factor and conversion efficiency are listed in Table 5. The conversion efficiency is increased with the incident photon power (100 mW/cm^2) for ZIST thin films due to an increase (J_{sc}) as a result of the decrease in the optical energy gap [40]. However, there is a rise in the value of (V_{OC}), which will increase the absorption coefficient, roughness, concentration of carriers.

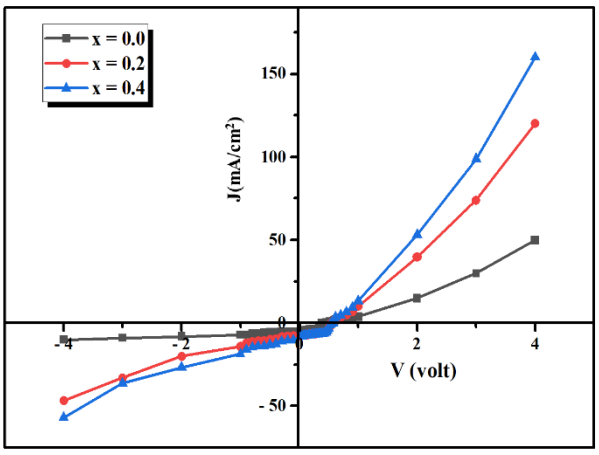

Fig. 4. I-V characteristic under illumination of a n-ZIST/p-Si solar cell at RT.

Table 5. I-V factors under light of the n-ZIST/p-Si solar cell at RT.

Thickness (500) nm	V_{oc} Volt	J_{sc} mA/cm^2	V_m Volt	J_m mA/cm^2	F.F	η %
ZIST (x = 0.0)	0.3757	4.76	0.3159	3.3	0.582	1.04
ZIST (x = 0.2)	0.56	7.4	0.45	5.5	0.597	2.47
ZIST (x = 0.4)	0.585	8	0.48	6.2	0.635	2.97

4. Conclusions

$ZnIn_2(Se_{1-x}Te_x)_4$ (ZIST) chalcopyrite semiconductor thin films at various contents (x = 0.0, 0.2, & 0.4) were successfully prepared by thermal evaporation technique at RT. It was found that increasing x content improved the physical properties of ZIST thin film. The XRD revealed a tetragonal structure of a polycrystalline in all films. As the x content increased, the crystallites size grew from 10.4 to 30.46 nm, and the optical gap decreased from 2 eV to 1.6 eV. Absorption coefficient also increased from 2.41×10^4 to 4×10^4 cm^{-1} which makes them suitable thin films for electro-optical applications, especially solar cell. Hall measurements established that all films have n type conductivity. I-V characteristic under light power of 100 mW/cm^2 shows that n-ZIST/p-Si solar cell heterojunction has the highest conversion efficiency (2.97%) and fill factor (0.635) at x content equal to 0.4.

References

[1] Y. Jin, M. Zhang, L. Song, M. Zhang, Small, **19** (10), 2206081(2023); https://doi.org/10 .1002/smll.202206081.
[2] W. R. Fahrner, Amorphous silicon/crystalline silicon heterojunction solar cells, Springer, Heidelberg New York Dordrecht London, 3 (2013); https://doi.org/10 .1002/smll.202206081.
[3] R. N. Gayen, S. R. Bhattacharyya, J. Phys. D. Appl. Phys., **49** (11), 115102 (2016); https://doi .org/10.1088/0022-3727/49/11/115102.
[4] S. M. Sze, Y. Li, K. K. Ng, Physics of semiconductor devices, John wiley & sons, Hoboken, New Jersey,124 (2021).
[5] F. J. Garcia, M. S. Tomar, Thin Solid Films, **69** (2),137(1980); https://doi.org/10.1016/0040-6090(80)90028-0.
[6] M. Isik, H. H. Gullu, S. Delice, N. M. Gasanly, M. Parlak, J. Mater. Sci. Mater. Electron., **30**, 9356 (2019); https://doi.org/10.1007/s10854-019-01265-5.
[7] M. M. El-Nahass, A. A. Attia, H. A. M. Ali, G. F. Salem, M. I. Ismail, J. Electron. Mater., **47**, 2739 (2018); https://doi.org/10.1007/s11664-018-6126-8.
[8] D. K. Dhruv, B. H. Patel, S. D. Dhruv, P. B. Patel, U. B. Trivedi, N. Agrawal, Mater. Today Proc., **84**, 1(2023); https://doi.org/10.1016/j.matpr.2023.01.199.
[9] S. P. Yadav, P. S. Shinde, K. Y. Rajpure, C. H. Bhosale, J. Phys. Chem. Solids, **69** (7), 1747 (2008); https://doi.org/10.1016/j.jpcs.2007.12.012.
[10] E. Fortin, F. Raga, Solid State Commun., **14** (9), 847 (1974); https://doi.org/10.1016/0038-1098(74)90148-3.
[11] P. Babu, M. V Reddy, N. Revathi, K. T. R. Reddy, J. Nano-and Electron. Phys., **3** (1), 85 (2011).
[12] M. Sugiyama, A. Kinoshita, A. Miyama, H. Nakanishi, S. F. Chichibu, J. Cryst. Growth, **310** (4), 794 (2008); https://doi.org/10.1016/j.jcrysgro.2007.11.172.
[13] A. C. Pawar, A. V Kokate, P. S. Raut, J. A. Borase, B. G. Wagh, H. R. Kulkarni, Material Science Research India, **7** (1), 295 (2010); http://dx.doi.org/10.13005/msri/070141.
[14] I. A. Mamedova, AJP Fiz., **27** (2), 8 (2021).
[15] T. A. Hendia, L. I. Soliman, Thin Solid Films, **261**(1–2), 322 (1995); https://doi.org/10.1016 /S0040-6090(94)06488-1.
[16] M. A. Repins, B. E. Contreras, C. DeHart, J. Scharf, CL Perkins, B. To, R. Noufi, Prog. Photovoltaics, **16** (3), 235 (2008); https://doi.org/10.1002/pip.822.
[17] D. K. Dhruv. B. H. Patel, Significance, **3** (5), 9 (2015); http://doi.org/10.17148 /IJIREEICE. 2015.3503.
[18] S. Mora, C. Paorici, N. Romeo, J. Appl. Phys., **42** (5), 2061(1971); https://doi.org/10.1063/1 .1660487.
[19] N. Romeo, A. Dallaturca, R. Braglia, G. Sberveglieri, Appl. Phys. Lett., **22** (1), 21(1973); https ://doi.org/10.1063/1.1654457.
[20] A. G. Abdullayev, T. G. Kerimova, M. G. Kyazumov, A. S. Khidirov, Thin Solid Films, **190** (2), 309 (1990); https://doi.org/10.1016/0040-6090(89)90920-6.

[21] H. H. Güllü, E. Coşkun, M. Parlak, Optik (Stuttg)., **144**, 603(2017); https://doi.org/10.1016/j . ijleo.2017.06.106.
[22] D. K. Dhruv, A. Nowicki, B. H. Patel, V. D. Dhamecha, Surf. Eng., **31** (7), 556 (2015); https: //doi.org/10.1179/1743294415Y.0000000001.
[23] S.-H. Choe, Curr. Appl. Phys., **9** (1), 1(2009); https://doi.org/10.1016/j.cap.2007.10.083.
[24] I. H. Khudayer, B. H. Hussien, Ibn AL-Haitham J. Pure Appl. Sci., **29** (2), 41(2017).
[25] B. K. H. Al-Maiyaly, Ibn AL-Haitham J. Pure Appl. Sci., **29** (3), 14 (2017).
[26] B. D. Cullity, "Elements of X-ray Diffraction". Addison-Wesley Publishing, Inc.Reading, Massachusetts, 259 (1956).
[27] R. H. Athab, B. H. Hussein, Ibn AL-Haitham J. Pure Appl. Sci., **35** (4), 45 (2022); https://doi. org/10.30526/35.4.2868.
[28] M. S. Hossain, S. Ahmed, Results Mater., **20**, 100492 (2023); https://doi.org/10.1016/ j.rinma. 2023.100492.
[29] J. I. Pankove, "Optical processes in semiconductors". Dover Publications, Inc. New York, 36 (2010).
[30] B. H. Hussein, I. H. Khudayer, M. H. Mustafa, A. H. Shaban, Prog. Ind. Ecol. An Int. J., **13** (2) ,173 (2019); https://doi.org/10.1504/PIE.2019.099358.
[31] B. H. Hussein, S. H. Mahdi, S. A. Makki, B. K. H. Al-Maiyaly, Energy Procedia, **157**, 100 (2019); https://doi.org/10.1016/j.egypro.2018.11.169.
[32] R. H. Athab, B. H. Hussein, Digest Journal of Nanomaterials and Biostructures, **17** (4), 1173-1180 (2022); https://doi.org/10.15251/DJNB.2022.173.1173.
[33] R. H. Athab, B. H. Hussein, Chalcogenide Lett., **20** (2), 91 (2023); https://doi.org/10.15251/CL.2023.202.91.
[34] Bahjat B. Kadhim, Imad H. Khaleel, Bushra H. Hussein, Kareem Ail Jasim, Auday H. Shaban, Bushra K.H. AL-Maiyaly, Shatha H. Mahdi, AIP Conference Proceedings, 1968: 030054, (2018); https://doi.org/10.1063/1.5039241.
[35] B. K. H. Al-Maiyaly, B. H. Hussein, A. A. Salih, A. H. Shaban, S. H. Mahdi, I. H. Khudayer, AIP Publishing, **1968** (1), 1 (2018); https://doi.org/10.1063/1.5039233.
[36] D. K. Dhruv, B. H. Patel, D. Lakshminarayana, Mater. Res. Innov., **20** (4), 285 (2016); https: //doi.org/10.1080/14328917.2015.1131919.
[37] B. H. Hussein, H. K. Hassun, NeuroQuantology,**18** (5), 77 (2020); https://doi.org/10.14704/ nq .2020.18.5.NQ20171.
[38] S. N. Sobhi, B. H. Hussein, Ibn AL-Haitham J. Pure Appl. Sci., **35** (3), 16 (2022); https://doi.org /10.30526/35.3.2824 .
[39] F. Yu, X. Meng, J. Cheng, J. Liu, Y. Yao, J. Li, J. Alloys Compd., **797**, 940 (2019); https:// doi.org/10.1016/j.jallcom.2019.05.238.
[40] B. H. Hussein, H. K. Hassun, B. K. Maiyaly, S. H. Aleabi, J. Ovonic Res, **18** (1), 37 (2022); https://doi.org/10.15251/JOR.2022.181.37.